Reduced Electron Thermal Transport in Low Collisionality H-mode Plasmas in DIII-D and the Importance of Small-scale Turbulence

L. Schmitz,[1] C. Holland,[2] T.L. Rhodes,[1] G. Wang,[1] L. Zeng,[1] A.E. White, [3]
J.C. Hillesheim[1], W.A. Peebles,[1] S. Smith,[4] R. Prater,[4] G.R. McKee,[5] W.M. Solomon,[6]
K.H. Burrell,[4] E.J. Doyle,[1] J.C. DeBoo,[4] M.E. Austin,[7] J.S. deGrassie,[4] and C.C. Petty[4]

[1]University of California, Los Angeles, Los Angeles, California 90095-7799, USA
[2]University of California, San Diego, La Jolla, California 92093, USA
[3]Massachsetts Institute of Technology, Cambridge, Massachusetts 02139, USA
[4]General Atomics, San Diego, California 92186-5608, USA
[5]University of Wisconsin-Madison, Madison, Wisconsin 53706, USA
[6]Princeton Plasma Physics Laboratory, Princeton, New Jersey 08543-0451, USA
[7]University of Texas at Austin, Austin, Texas 78712-1047, USA

e-mail contact of main author: lschmitz@ucla.edu

Abstract. The first systematic investigation of core electron thermal transport and the role of local ion temperature gradient/trapped electron mode/electron temperature gradient (ITG/TEM/ETG)-scale core turbulence is performed in high temperature, low collisionality DIII-D H-mode plasmas. Taking advantage of the unique set of DIII-D turbulence and profile diagnostics, experimentally determined L-mode and H-mode turbulence wavenumber spectra are directly contrasted for the first time with nonlinear gyrokinetic simulation results. Core ITG/TEM-scale turbulence is substantially reduced/suppressed by $\boldsymbol{E}\times\boldsymbol{B}$ shear promptly after the L-H transition, resulting in reduced electron thermal transport across the entire minor radius. For small $k_\theta\rho_s$, both experiment and nonlinear gyrokinetic (GYRO) simulations show density fluctuation levels increasing with $k_\theta\rho_s$ in H-mode (r/a=0.6), in contrast to ITG/TEM-dominated L-mode plasmas. GYRO simulations also indicate that a significant portion of the remaining H-mode electron heat flux results directly from residual short-scale TEM/ETG turbulence. These studies are performed at ITER-relevant collisonality ($\nu_e^* \sim 0.05$, $r/a \leq 0.6$) and address transport in electron heat-dominated regimes, thought to be important in ITER due to α-particle heating.

1. Introduction

Electron thermal transport is intrinsically a multi-scale phenomenon, and can be driven by turbulence in the ion temperature gradient/trapped electron mode (ITG/TEM) wavenumber range as well as in the short-scale electron temperature gradient (ETG) mode range. With the discovery of radially elongated structures in ETG turbulence [1], it has been conjectured that short-scale turbulence can contribute substantially to electron thermal transport. Multi-scale gyrokinetic simulations have indicated that ETG-scale modes persist in the presence of ITG/TEM scale turbulence even if the ETG mode is linearly stable. This effect has been attributed to nonlinear cascading from low towards higher wavenumbers [2,3]. However, in these simulations electron transport has been predicted to be still predominantly driven by the larger-scale modes. A different situation arises if ITG/TEM modes are close to marginal stability or suppressed by $\boldsymbol{E}\times\boldsymbol{B}$ shear. In this case, similar simulations and also more recent gyrokinetic work [4] indicate that a substantial part of electron thermal transport can result directly from small-scale ETG turbulence. In the presence of unstable ETG modes, a scale separation between electron and ion transport can result, with the electron transport dominated by the spectral range $k\rho_s > 1$, where $\rho_s = c_s m_i / eB_t$ is the ion sound gyroradius with $c_s = \sqrt{kT_e / m_i}$).

We report here the first experimental measurements of local wavenumber spectra of density fluctuations in L- and H-mode in high temperature, low collisionality plasmas, where electron and ion channel transport are esssentially decoupled. Doppler backscattering (DBS) [5,6], allows local measurements of relative density fluctuation levels versus poloidal wavenumber and hence provides data for direct comparison with wavenumber spectra obtained from quasilinear gyro-fluid calculations or gyrokinetic simulations. These

measurements span the ITG wavenumber range up to the (transport-relevant) lower ETG range ($0.3 \le k\rho_s \le 6$). Measurements as well as linear stability calculations indicate that ITG/TEM-scale density fluctuations are substantially reduced across the minor radius in H-mode in these plasmas. Electron thermal transport is reduced after the L-H transition as well across the entire minor radius. Experimental evidence indicates substantial flattening of the wavenumber spectrum in H-mode, hence supporting the conjecture that short-wavelength modes contribute to H-mode core electron thermal transport.

2. Turbulence and Transport Evolution Across the L-H transition

Figure 1 shows the time evolution of density and electron temperature fluctuations, the ***E×B*** shear, and the linear instability growth rates in a counter-injected plasma, where the L- to H-mode transition is induced by stepping the neutral beam power from about 5 MW to 7.5 MW. At the L-H transition, the line-averaged density increases from 1.6×10^{13} cm^{-3} to 2.6×10^{13} cm^{-3}. Core density fluctuations in the ITG wavenumber range [Fig. 1(a)], measured by Doppler backscattering and beam emission spectroscopy (BES), decrease substantially across the transition, indicated by the drop in D_α line intensity [Fig. 1(e)]. In addition, core electron temperature fluctuations from correlation electron cyclotron emission radiometry (CECE [7]), are reduced within ~10 ms of the L-H transition (r/a=0.7) [8]. Intermediate scale density fluctuations ($k_\theta\rho_s$=2, r/a=0.4, measured by DBS) are also reduced by a factor of ~2.5–3 at the transition, after a gradual decrease prior to the transition [Fig. 1(b)]. This initial decrease, also seen in the BES data [Fig. 1(a)], is likely related to increasing shear after the step-up in neutral beam power. Figure 1(c) shows a comparison of the (normalized) maximum linear instability growth rates in the ITG/TEM range ($k_\theta\rho_s\le2$) and the ETG range ($k_\theta\rho_s>2$) with the Waltz-Miller ***E×B*** quench rate

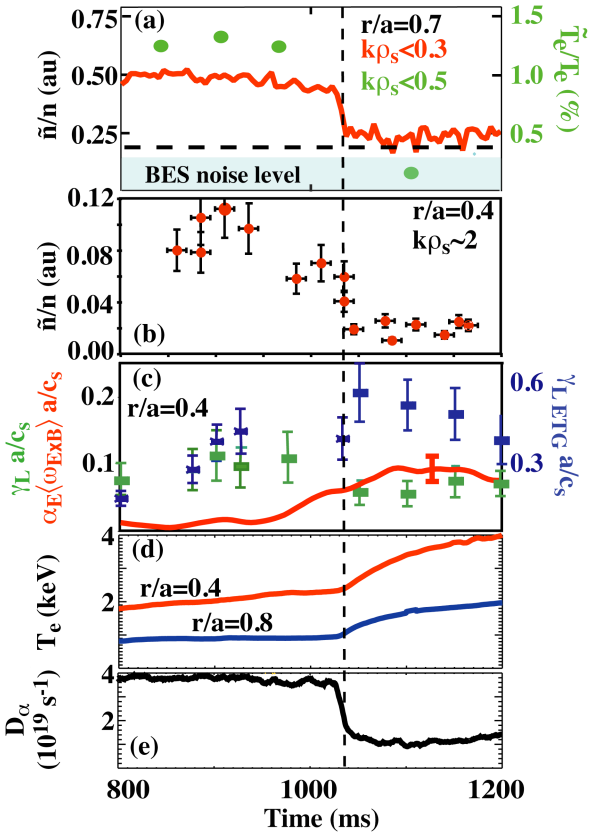

FIG. 1. (a) ITG-scale density and electron temperature fluctuation (r/a=0.7); dashed line: CECE detection limit; (b) density fluctuation level for $k\rho_s$~2); (c) comparison of maximum linear ITG/TEM growth rate ($k\rho_s$<2) and ETG growth rate (from TGLF) with the ExB shearing rate (r/a=0.4); (d,g) time evolution of local electron temperature; (e) D_α signal.

$$\alpha_E(a/c_s)\omega_{ExB} = \alpha_E(a/c_s)\left\langle\left[(RB_\theta)^2/B_t\right](\partial/\partial\psi)(E_r/RB_\theta)\right\rangle \quad ,$$

evaluated from charge exchange recombination (CER) data. Here, α_E~$0.3(\kappa)^{1/2}$ is the quench factor determined empirically by systematic variations of the shearing rate in gyrokinetic (GYRO [9]) simulations [10], and κ is the local flux surface elongation. Instability growth rates are calculated using the trapped gyro-Landau fluid code (TGLF) [11,12].

Around the time of the L-H transition the quench rate exceeds the maximum linear ITG/TEM growth rate in the core plasma (shown for r/a=0.4). In contrast, the ETG growth rate always remains much above the shearing rate. It should be noted that the plasma in H-mode is close to marginal stability as the maximum linear ITG/TEM growth rate remains close to the quench rate.

At the L-H transition, the electron temperature starts increasing first near the edge (pedestal formation), but also very rapidly in the core plasma [Fig. 1(d)]. The time evolution of the electron temperature and the electron heat diffusivity is examined in more detail in Fig. 2. Electron cyclotron emission (ECE) data indicate a substantial increase at the L-H transition (1030 ms) across the minor plasma radius [Fig. 2(a)]. Figures 2(b-d) show an expanded view of the time evolution of the electron heat diffusivity (evaluated using time-dependent TRANSP transport modeling) and the electron temperature across the transition time, indicated by the drop in the D_α signal. The electron thermal diffusivity shows a substantial reduction in the core plasma across the minor radius within 10 ms of the transition [Fig. 2(b)], implying globally reduced electron thermal transport.

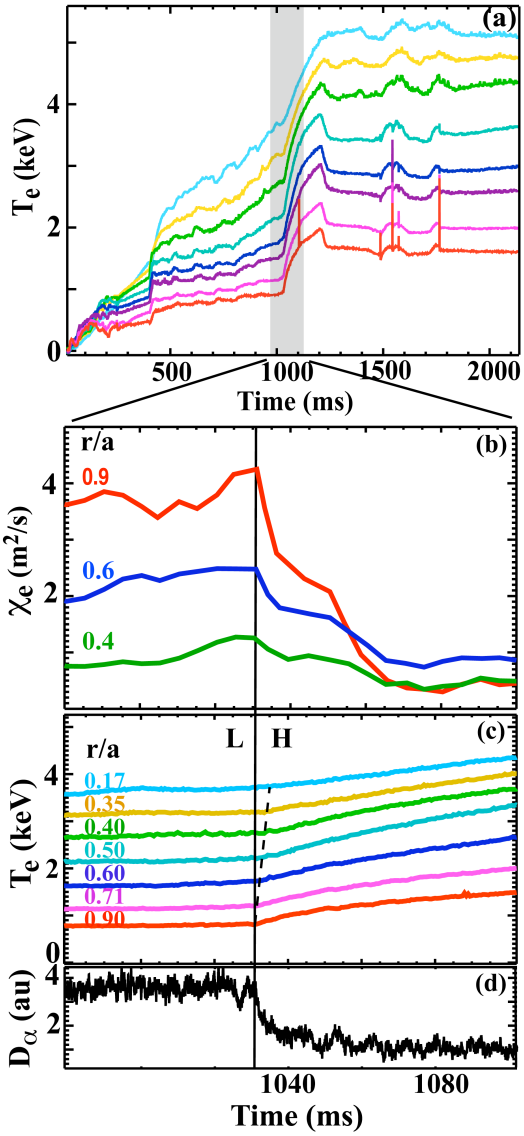

FIG. 2. (a) Time evolution of electron temperature (ECE data); the shaded region indicates the time window of the L-H transition [expanded in (b,c,d)]; (b) evolution of electron thermal diffusivity across the L-H transition; (c) electron temperature time evolution (expanded view); (d) D_a signal indicating the L-H transition time.

Figure 3 shows the radial profiles of electron and ion temperatures, and plasma density in L- and H-mode. In addition to pedestal formation evident in the electron temperature, ion tempera-

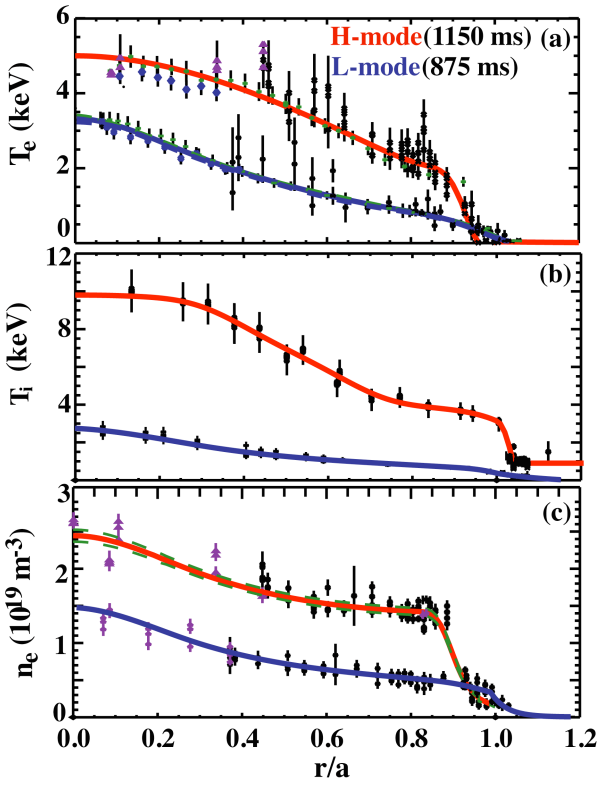

FIG. 3. Radial profiles of (a) electron temperature; (b) ion temperature, and (c) electron density in L- and H-mode.

ture and plasma density profiles, an internal ion temperature barrier is observed to form in H-mode at $0.3 \le r/a \ge 0.6$ [13,14]. In addition to the very substantial improvement in core ion confinement, the electron temperature more than doubles for $r/a > 0.3$. In H-mode, the electron to ion temperature ratio is $T_e/T_i \sim 0.5\text{-}0.7$, depending on radius for the results discussed here.

Figure 4(a) shows normalized density fluctuation levels (measured by DBS, 1125–1175 ms) and demonstrates that ITG-scale fluctuations are reduced across the entire minor radius in H-mode, with the most substantial reduction (more than an order of magnitude) occurring in the plasma core ($0.3 \le r/a \le 0.6$), in addition to the reduction associated with pedestal formation which has been documented previously [15]. We ascribe the dramatic reduction in core ion and electron transport in H-mode, and the formation of the core ion transport barrier, to this turbulence reduction. In addition to reduced ITG-scale turbulence, substantial reductions in intermediate-scale and shorter-scale turbulence are seen in the inner core. These reductions primarily affect the electron channel. Figure 4(b) shows DBS measurements of normalized density fluctuation levels at $k_\theta \rho_s = 2$, in the upper TEM range. The observed reduction is about a factor of three across the outer core plasma and more substantial in the inner core. Also shown is a profile of shorter-scale fluctuation in the ETG range in H-mode ($k\rho_s = 4$). No comparison data for L-mode are given, since this normalized wavenumber range is not accessible by the DBS diagnostic in L-mode due to the lower electron temperature.

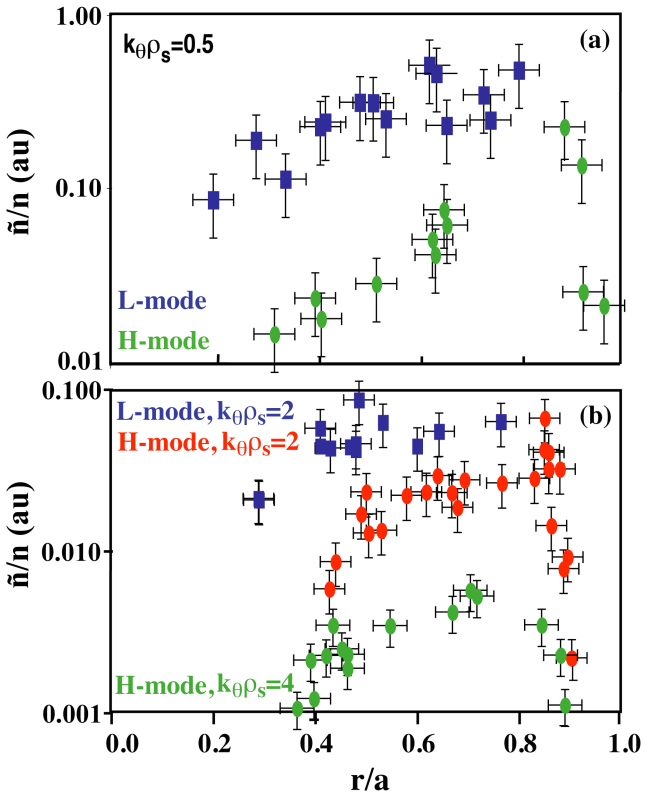

FIG. 4. Radial profiles of density fluctuation levels in L- and H-mode: (a) ITG-scale, and (b) intermediate and ETG-scale fluctuations.

3. Turbulence Wavenumber Spectra, Linear Stability and Initial Gyrokinetic Simulation Results

Figure 5(a,c) shows wavenumber spectra of core density turbulence, measured by DBS. In L-mode, spectra are best described by an exponential dependence on $k_\theta \rho_s$ ($\tilde{n}/n \sim \exp(-\zeta k_\theta \rho_s)$ with ζ=1.45-1.7). This scaling is similar to the scaling observed previously in the TORE SUPRA tokamak [16]. In L-mode the wavenumber range accessible by DBS is limited to $k_\theta \rho_s \sim 2$ due to the lower electron temperature. In contrast, in H-mode, where the electron temperature is much higher, $k_\theta \rho_s \le 6$ can be accessed. Density fluctuation levels are significantly reduced at low and intermediate wavenumber range (ITG/TEM-scale). For r/a=0.4 the wave-number spectra are substantially flatter in this spectral region. For r/a=0.6 ITG/TEM-scale fluctuations are also very substantially reduced below $k_\theta \rho_s \sim 1$. In the ETG range, fluctuation levels decay roughly exponentially at higher wavenumbers *($k_\theta \rho_s > 4$)*. For r/a=0.6, the data indicate a peak in the intermediate (TEM) wavenumber range *($k_\theta \rho_s \sim 1$)* and a local maximum at $k_\theta \rho_s \sim 2.5$, in the lower ETG range. Comparing linear instability growth rates from TGLF with Miller-Waltz quench rates [Figs. 5(b,d)] we find that the

wavenumber range of reduced large/intermediate-scale turbulence is well predicted by the wavenumber range where the quench rate $a/c_s\alpha_E\langle\omega_{E\times B}\rangle$ exceeds the normalized linear growth rate. In Fig. 5(b,d) we plot $a/c_s[\gamma_L - \alpha_E\langle\omega_{ExB}\rangle]$ versus the normalized wavenumber $k\rho_s$; the suppression range corresponds to negative ordinate values.

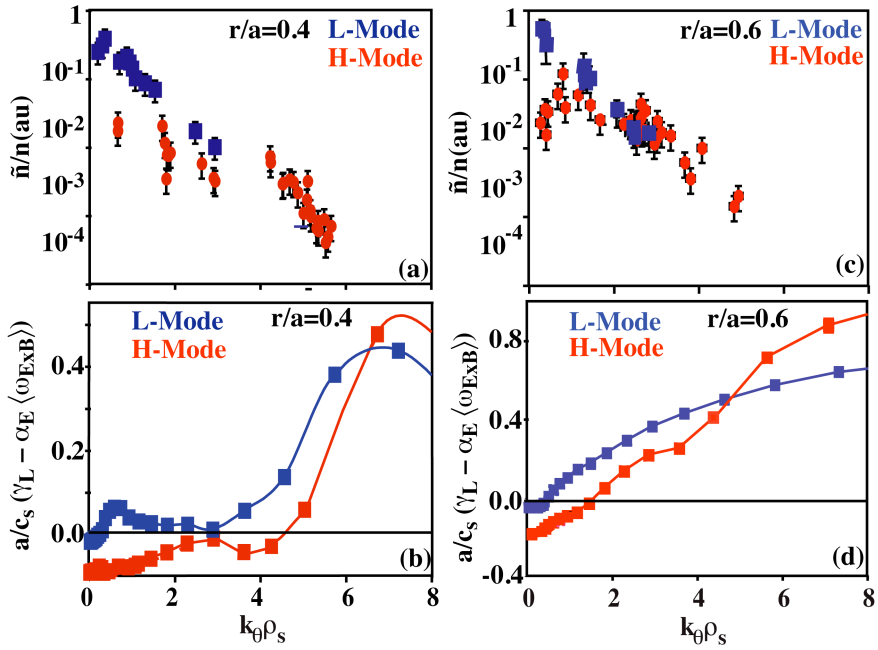

FIG. 5. Density fluctuation wave-number spectra (L/H-mode) at r/a=0.4 (a) and r/a= 0.6 (c); corresponding linear growth rates and ExB quench rates (b,d).

Figure 6 shows the wavenumber spectrum of density fluctuations predicted by a preliminary, local, nonlinear GYRO simulation, for the early H-mode phase of shot #131912 (r/a=0.6, t = 1100 ms). This is a true multiscale simulation evolving fully gyrokinetic electrons, deuterium and carbon ions. Electromagnetic effects, electron-ion collisions (pitch-angle scattering), and equilibrium ***E×B*** shear are included. Forty toroidal modes were used to span the wavenumber range $0 \le k_\theta\rho_s \le 21.3$, with a resolution of $\Delta k_\theta\rho_s = 0.27$; the radial grid resolution was $0.065\rho_s$ and physical radial domain $L_x = 21\rho_s$. In order to run the simulation long enough to obtain well-converged statistics in the fully saturated state, a reduced ion to electron mass ratio of $(M/m)^{1/2} = 40$ (as opposed to the physical value of 60.6) was used. This value was chosen based on previous studies which found that this value yielded the optimal trade-off in physical fidelity and computational cost [3,4]. Even with the reduced mass ratio and relatively small box size, approximately 90,000 cpu-hours were required. In Fig. 6(a), the density fluctuation spectrum integrated over k_r falls off as $\tilde{n}\sim(k_\theta\rho_s)^{-1.8}$ at high k_θ. The spectrum labeled k_r=0 takes into account the instrumental DBS sensitivity which intrinsically detects modes with k_r=0 [6]. In contrast to the integrated spectrum, for k_r=0 the spectrum falls off as as $\tilde{n}\sim(k_\theta\rho_s)^{-2.7}$. This difference is related to the properties of the (anisotropic) 2-D wavenumber spectrum [Fig. 6(c)]. Comparing the decay of the spectral density with poloidal normalized wavenumber for k_r=0 and the spectral density decay averaged over k_r, it is obvious that the latter exhibits a more gradual reduction, as described earlier [17]. Both the density fluctuation wavenumber spectrum and the electron energy flux spectrum exhibit a peak near $k_\theta\rho_s\sim5$, in the ETG range, indicating that small-scale fluctuations are expected to dominate electron heat transport in H-mode.

Since only a single fixed gradient GYRO simulation has been conducted to date, a quantitative assessment of code-experiment agreement is premature. A proper comparison

would account for the significant sensitivities that the ratio of ITG/TEM and ETG transport exhibits to background gradients and ***E×B*** shear, which have not yet been fully assessed. Given this caveat, we note that several features of the experimental wavenumber spectrum [Fig. 5(c)] are however reflected in the present GYRO simulation. The density fluctuation level increases with poloidal wavenumber in the low-k range ($1 \le k_\theta \rho_s \le 2$) in both the experimental and the GYRO spectrum. Both spectra exhibit local maxima at intermediate k_θ in the TEM and in the lower (transport-relevant) ETG range, at $k_\theta \rho_s \sim 1$ and $k_\theta \rho_s \sim 2.5$ in the experiment, and at $k_\theta \rho_s \sim 1$ and $k_\theta \rho_s \sim 5$ in the GYRO result, although the ETG peak is much more pronounced in the GYRO spectrum. This behavior is entirely different from the L-mode experimental spectra reported here and in previous gyrokinetic simulations for beam-heated [3] and ECH L-mode plasmas [19] where the density fluctuation spectrum was observed to peak at low k_θ.

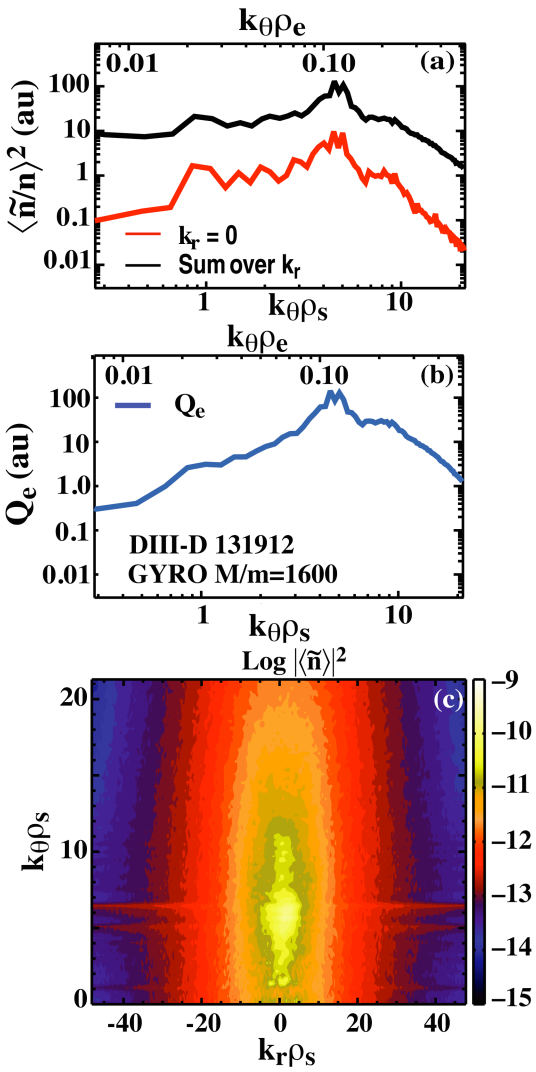

FIG. 6. GYRO nonlinear simulations of early H-mode phase (r/a=0.6); (a) Wavenumber spectrum of squared density fluctuations, for k_r=0 and integrated over the entire k_r spectrum; (b) electron thermal flux spectrum, (c) 2-D wavenumber spectrum of squared density fluctuations.

4. Dependence of Turbulence and Electron Transport on Electron/Ion Temperature Ratio

To investigate transport dependence on the ratio of T_e/T_i, central ECH has been added during H-mode to increase the electron temperature. ELM-free operation is maintained as the H-mode plasmas described above develop into quiescent (ELM-free) QH-mode plasmas [20] after the initial ELM-free H-mode phase. Figure 7 shows the radial electron temperature profile, the electron thermal diffusivities, and the density and electron temperature fluctuation levels before (1705 ms) and during (2625 ms) ECH application ($P_{ECH} \sim 2.7$ MW). A substantial increase in electron temperature across the minor radius has been achieved, resulting in $T_e/T_i \sim 1$ at r/a=0.6 and $T_e/T_i > 1$ for $r/a < 0.5$. Fig. 7(b) shows increased electron thermal diffusivity during ECH across the minor radius. It is notable that low-k and intermediate-k density fluctuations are not changed substantially during ECH [Fig. 7(c)], while low-k electron temperature fluctuations increase very substantially at CECE-accessible radii [Fig. 7(d), r/a>0.6]. TGLF linear stability calculations for r/a=0.6 [Fig. 7(e)] indicate that low-k TEM-modes dominate during ECH with growth rates much larger than the ***E×B*** quench rate, which is reduced with ECH. It should be noted that the ion temperature central barrier [Fig. 3(b)] is absent during ECH and the ion temperature and ion temperature gradient (not shown here) are lower due to increased ion thermal transport. The local electron

temperature gradient and density gradient scale lengths were kept constant at r/a=0.6 with and without ECH (R/L_{Te}~5.5, R/L_n~2.2). The dominance of TEM modes during ECH is likely related to the increased T_e/T_i ratio and the reduced ion temperature gradient scale length (R/L_{Ti}~4.2 before ECH, R/L_{Ti}~1.4 with ECH), as indicated by sensitivity studies of the TGLF linear growth rate to different parameters.

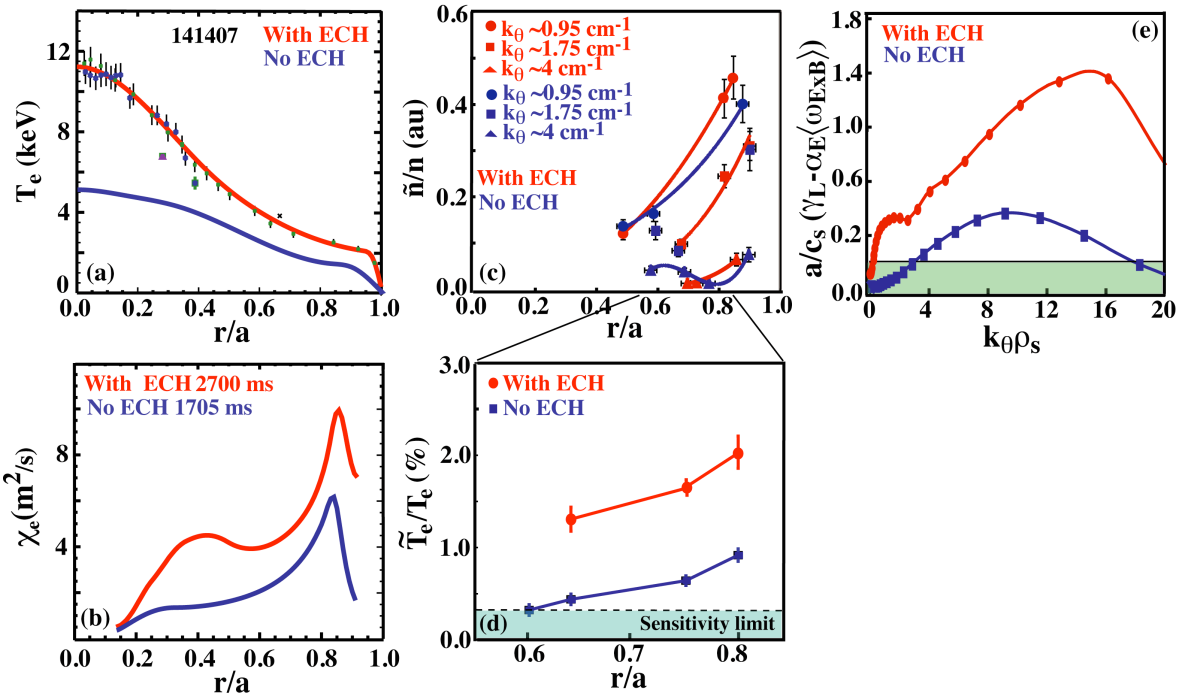

FIG. 7. (a) Electron temperature profiles with/without ECH; (b) electron thermal diffusivities; (c) density fluctuation levels from DBS for the ITG./TEM range; (d) electron temperature fluctuation levels from CECE; (e) Difference of linear growth rate (from TGLF) and quench rate (r/a=0.6).

5. Summary and Discussion

We have for the first time provided detailed turbulence measurements and investigated the connection between multi-scale turbulence and electron transport in high temperature H-mode plasmas. These plasmas have ITER-relevant core plasma collisionality, and are particularly well suited to study electron transport physics since the electron and ion transport channels are decoupled. Evidence of significantly reduced large-scale and intermediate-scale core turbulence across the plasma minor radius has been presented. The observed reduction is consistent with quenching of ITG/TEM–scale core turbulence by ***E×B*** shear. For r/a=0.4, turbulence suppression in the inner core plasma occurs for wavenumbers $k_\theta\rho_s$≤3…4, in agreement with the range where the ***E×B*** quench rate exceeds the linear instability growth rate. It has been shown that ITG/TEM turbulence remains close to marginal stability in H-mode where the quench rate is approximately equal to the maximum linear growth rate. At r/a=0.6, turbulence suppression in a more limited wavenumber range ($k_\theta\rho_s \leq 1$) has been observed, again in agreement with linear stability calculations. Decreased electron thermal diffusivity is observed across the plasma minor radius concomitantly with turbulence reduction. The turbulence wavenumber spectra in L-mode show an exponential dependence on normalized wavenumber. In H-mode, the wavenumber spectrum flattens at intermediate wavenumbers, and is characterized by increased high-k fluctuations in the ETG range. At

high wavenumber, the H-mode fluctuation levels again decrease approximately exponentially with normalized wavenumber. These results represent the first experimental evidence of flat/inverted wavenumber spectra in the ITG range, which have been so far only observed in numerical simulations [4]. We have performed initial GYRO calculations, which reflect qualitatively some of the features seen in the experimental spectra. Flux-matched quasi-linear calculations using the TGLF code will be used in preparation for flux-matched GYRO runs [16], to enable quantitative comparisons of the experimentally observed and calculated density fluctuation spectra.

Transport dependence on the electron- to ion temperature ratio is important for burning plasmas which are dominated by α-particle heating and which are expected to have $T_e \geq T_i$. Turbulence data for a range of T_e/T_i values, including $T_e/T_i \geq 1$, have been obtained in recent experiments with very similar plasmas by adding up to 2.7 MW of central ECH (presently under analysis). Substantially increased low-k electron temperature fluctuations with growth rates above the $\boldsymbol{E}\times\boldsymbol{B}$ quench rate are found. From linear stability analysis, low/intermediate-k TEM mode activity is found to dominate the growth rate spectrum. We will report more detailed results of transport analysis and linear and nonlinear turbulence modeling from these plasmas in the future.

This work was supported by the US Department of Energy under DE-FG02-08ER54984, DE-FG02-07ER54917, DE-FC02-93ER54186, DE-FC02-04ER54698, DE-FG02-89ER53296, DE-FG02-08ER54999, DE-AC02-09CH11466, DE-FG03-97ER54415, and NS53250. This research used resources of the Oak Ridge Leadership Computing Facility at Oak Ridge National Laboratory, which is supported by the US Department of Energy under DE-AC05-00OR22725.

References

[1] JENKO, F. and DORLAND, W., Phys. Rev. Lett. **89** (2002) 225001
[2] CANDY, J., *et al.,* Plasma Phys. Control. Fusion **49** (2007) 1209
[3] WALTZ, R.E., *et al.,* Phys. Plasmas **14** (2007) 056116
[4] GOERLER, T. and JENKO, F., Phys. Rev. Lett. **100** (2008) 185002
[5] HIRSCH, M., *et al.,* Plasma Phys. Control. Fusion **43** (2001) 1641
[6] HILLESHEIM, J., *et al.,* Rev. Sci. Instrum. **80** (2009) 083507
[7] WHITE, A.E., *et al.,* Rev. Sci. Instrum. **79** (2008) 103505
[8] SCHMITZ, L., *et al.,* Phys. Rev. Lett. **100** (2008) 035002
[9] CANDY, J. and WALTZ, R.E., J. Comput. Phys. **186** (2003) 545
[10] KINSEY, J.E., *et al.,* Phys. Plasmas **15** (2008) 055908
[11] STAEBLER, G.M., *et al.,* Phys. Plasmas **12** (2005) 102508
[12] STAEBLER, G.M., *et al.*, Phys. Plasmas **14** (2007) 055909
[13] GREENFIELD, C.M., *et al.,* Phys. Rev. Lett. **86** (2001) 4544
[14] DOYLE, E.J., *et al.,* Plasma Phys. Control. Fusion **43** (2001) A95
[15] RETTIG, C.L., *et al.,* Nucl. Fusion **33** (1993) 643
[16] HENNEQUIN, P., *et al.,* Plasma Phys. Control. Fusion **46** (2004) B121
[17] HENNEQUIN, P., *et al.,* Nucl. Fusion **46** (2006) S771
[18] CANDY, J. and WALTZ, R.E., Phys. Rev. Lett. **91** (2003) 045001
[19] DeBOO, J.C., *et al.*, Phys. Plasmas **17** (2010), 056105
[20] BURRELL, K.H., *et al.*, Plasma Phys. Control. Fusion **44** (2002) A253